IOPscience iopscience.iop.org

Home Search Collections Journals About Contact us My IOPscience

THz generation from InN films due to destructive interference between optical rectification and photocurrent surge

This article has been downloaded from IOPscience. Please scroll down to see the full text article.

2010 Semicond. Sci. Technol. 25 015004

(http://iopscience.iop.org/0268-1242/25/1/015004)

View the table of contents for this issue, or go to the journal homepage for more

Download details:
IP Address: 129.187.254.46
The article was downloaded on 22/11/2010 at 13:59

Please note that terms and conditions apply.

Semicond. Sci. Technol. **25** (2010) 015004 (5pp) doi:10.1088/0268-1242/25/1/015004

THz generation from InN films due to destructive interference between optical rectification and photocurrent surge

Guibao Xu[1], Yujie J Ding[1,5], Hongping Zhao[1], Guangyu Liu[1], Muhammad Jamil[1], Nelson Tansu[1], Ioulia B Zotova[2], Charles E Stutz[3], Darnell E Diggs[3], Nils Fernelius[3], F Ken Hopkins[3], Chad S Gallinat[4], Gregor Koblmüller[4] and James S Speck[4]

[1] Department of Electrical and Computer Engineering, Lehigh University, Bethlehem, PA 18015, USA
[2] ArkLight, PO Box 2, Center Valley, PA 18034, USA
[3] Materials and Manufacturing Directorate, Air Force Research Laboratory, Wright-Patterson AFB, OH 45433, USA
[4] Materials Department, University of California, Santa Barbara, CA 93106, USA

E-mail: yud2@lehigh.edu

Received 16 September 2009
Published 8 December 2009
Online at stacks.iop.org/SST/25/015004

Abstract
We have investigated the characteristics of THz generation including the dependence of the output power and polarization on the incident angle and pump polarization from two series of InN films grown by plasma-assisted molecular beam epitaxy (PAMBE) and metal organic chemical vapor deposition (MOCVD), respectively. Following the analyses of our results, we have attributed the mechanism of the THz generation from these InN samples to the destructive interference between optical rectification and photocurrent surge. Under the average intensity of 176 W cm^{-2} for the subpicosecond laser pulses at 782 nm, the THz output powers were measured to be as high as 2.4 μW from the 220 nm InN film, with the output frequencies spanning the band from 300 GHz to 2.5 THz.

(Some figures in this article are in colour only in the electronic version)

Using ultrafast laser pulses, electro-optic materials [1, 2] can be used to efficiently generate broad THz pulses. Recently, it was demonstrated that ZnTe [3] and $LiNbO_3$ [4] can be used to generate high-power THz output pulses. Besides these two materials, other electro-optic materials such as InAs can also be used to generate THz pulses due to photocurrent surge [5] and resonance-enhanced optical rectification [6]. Recently, InN films were used to investigate the generation of THz pulses [7, 8]. Based on our recent result [9], even for the 700 nm thick InN film, the average output power reached 0.93 μW, which is comparable to other electro-optic materials, such as GaP, GaAs, InP and GaSe [10]. We attributed the mechanism for the THz generation in InN films primarily to resonance-enhanced optical rectification.

In this paper, we present our new results following our investigation of the THz generation from two series of InN films grown by PAMBE and MOCVD. Following our measurements of the dependence of the output power and polarization on the incident angle and pump polarization, we have observed the evidence on the destructive interference between optical rectification and photocurrent surge. Consistent with the previous result [9, 10], optical rectification is the primary mechanism for the THz generation. This is quite different from the mechanisms discussed in [7, 8]. The highest output power reached 2.4 μW from a 220 nm InN film, which is significantly higher than our previous result on the InN film with a comparable thickness. We have also confirmed the broadband nature of the THz output pulses through the measurement of the THz spectrum.

The two series of In-face InN films were grown by either PAMBE or MOCVD. The thicknesses of the InN films are

[5] Author to whom any correspondence should be addressed.

 © 2010 IOP Publishing Ltd Printed in the UK

Table 1. Summary of measurements made on two series of InN films.

InN grown by PAMBE				InN grown by MOCVD			
Sample ID	Electron density ($\times 10^{17}$ cm^{-3})	Mobility (cm^2 V s^{-1})	Highest output (μW)	Sample ID	Electron density ($\times 10^{19}$ cm^{-3})	Mobility (cm^2 V s^{-1})	Highest output (μW)
A	10.0	1639	1.68	1	3.90	324	1.53
B	8.53	1908	1.36	2	1.40	592	2.36
C	7.97	2069	1.88	3	3.90	324	1.48
D	9.63	1287	1.21	4	1.50	681	1.47
E	7.92	2279	1.42				

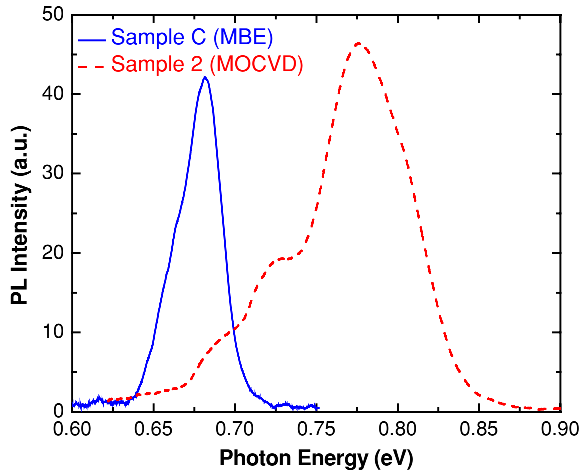

Figure 1. PL spectra of InN films being excited by a CW laser at 532 nm and 4.3 K.

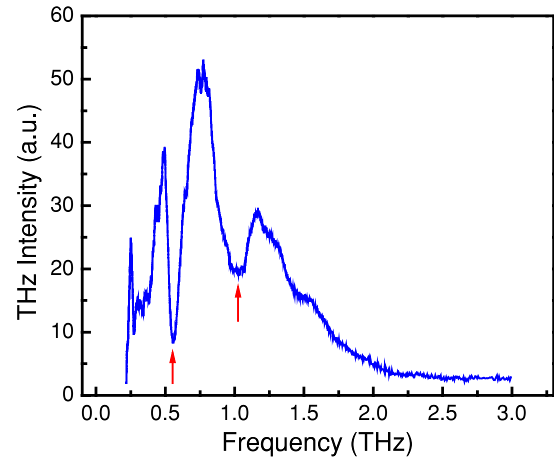

Figure 2. A typical frequency spectrum of THz radiation measured on one of the InN samples at room temperature.

either 1 μm or 220 nm. For each of the PAMBE-grown samples, prior to the deposition of the InN film, a semi-insulating (SI) GaN buffer layer was grown on a SI Fe-doped Ga-polar GaN template along the *c*-axis. The InN film was subsequently deposited with excess In at 460 °C. The accumulated In on the film surface was removed through etching by a HCl solution. On the other hand, for each of the MOCVD-grown samples, the InN film was deposited by pulsed MOCVD on an undoped GaN template grown on a *c*-plane sapphire substrate at 575 °C [11–13]. The densities of free electrons and mobilities obtained through Hall measurements are tabulated in table 1. The MOCVD growths of InN thin films were conducted using pulsed growth mode with TMIn and NH_3 as the In- and N-precursors, respectively. The use of pulsed MOCVD growth mode [11, 12] resulted in metallic-droplet-free narrow bandgap InN films grown on GaN/sapphire substrate. In the pulsed growth mode, NH_3 was constantly flown into the reactor with pulsing of the TMIn source during the InN growth. In the pulsing of the group-III precursor, the TMIn was sent into the reactor chamber for a 30-second pulse and followed by an 18-second pause (no TMIn) with a total cycle time of 48 seconds, corresponding to 62.5% duty cycle. The details of the pulsed MOCVD growth conditions for InN alloy can be obtained in [11] and [12].

Photoluminescence (PL) spectra of InN films excited by a CW laser at 532 nm were measured at 4.3 K, see figure 1. Apparently, these two series of the InN films exhibit different optical properties based on the PL spectra. Indeed, based on the spectra, we can deduce the bandgaps of the InN films to be 681 meV and 776 meV for the PAMBE-grown and MOCVD-grown InN films, respectively. Therefore, their bandgaps differ by 94.3 meV. In addition, there are two apparent bumps on the MOCVD-grown sample at 724 meV and 685 meV and a tail at 643 meV, respectively, see figure 1. They could be caused by the recombination of the carriers through defect states. According to figure 1, the half linewidths of the PL peaks determined at the half maxima on the high-energy edges are 38.5 meV and 12.8 meV for the MOCVD- and PAMBE-grown samples, respectively. The broadband THz pulses were generated from InN films by using a Ti:sapphire regenerative amplifier. Such an amplifier has an output central wavelength of 782 nm, and pulse duration of ~180 fs, and repetition rate of 250 kHz. The excitation laser beam was focused onto the InN side of each sample. The THz output was collimated along the propagation direction of the pump beam and subsequently focused onto a bolometer. Such a bolometer was calibrated in terms of the incoming THz powers. The spectrum of the THz output pulses was measured by a home-made THz spectrometer. In order to cover the entire frequency range, several gratings were used. One can see from figure 2 that the output frequencies span the range of from 300 GHz to 2.5 THz. One may notify the presence of the two pronounced dips in the spectrum at the frequencies of 550 GHz and 1.02 THz. Based on the HITRAN database, we have attributed these two peaks to the absorption of the water vapor present in the beam path.

In order to find out the highest output power, we have measured the dependence of the output power on the incident

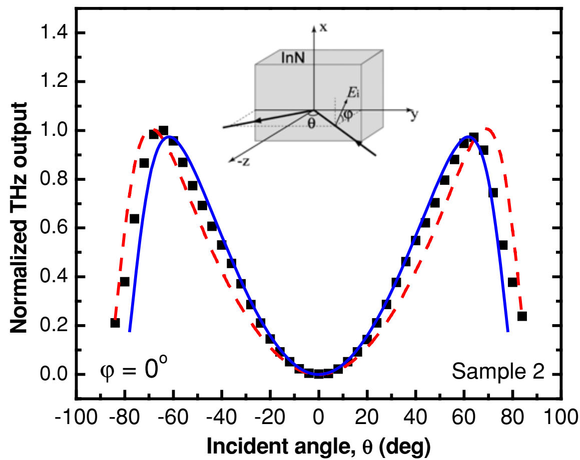

Figure 3. Normalized THz output power versus the incident angle of pump beam. Dots: experimental results. Solid curve: theoretical results by including optical rectification and photocurrent surge. Dashed curve: theoretical results without taking into consideration photocurrent surge. Inset: geometry for THz generation.

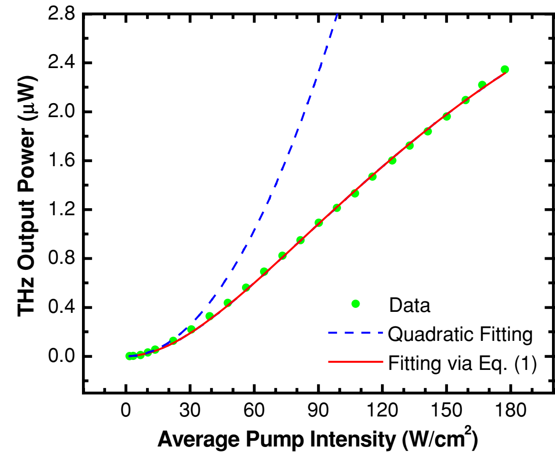

Figure 4. THz output power was measured as a function of pump intensity. Dots correspond to data points. Solid curve corresponds to nonlinear least-square fitting to all data points by using equation (1). Dashed curve designates theoretical result following quadratic least-square fitting to five data points from the low-intensity end.

angle. One can see from figure 3 that for a p-polarized pump beam ($\varphi = 0°$, see the inset in figure 3), the highest output power has occurred at the incident angle of $\theta \approx 64°$. Therefore, for reaching the highest output powers, we have set the incident angle of the p-polarized pump beam to 64°. At an average pump power of 1.06 W (the corresponding pump intensity of ~176 W cm^{-2}), the highest average THz output powers are well above 1 μW from all the InN samples, see table 1. Among them, the highest output power is measured to be 2.36 μW, generated from sample 2, which translates into a normalized conversion efficiency of 13.30 W cm^2 GW^{-1}. Compared with the highest output power generated from the similar thicknesses [9], this output power is about a factor of 12 higher, i.e. an improvement by one order of magnitude higher. When the pump intensity is lower than 30 W cm^{-2}, the dependence of the THz output power on the pump intensity is well fitted by a quadratic power dependence. However, for the pump intensities of higher than 30 W cm^{-2}, it appears to us that the dependence is close to the linear dependence, see figure 4.

Let us assume that the dependence of the THz output power (P_{THz}) on the pump intensity (I_{pump}) and the absorption coefficient for the THz wave (α_{THz}) is in the form of

$$P_{\mathrm{THz}} = C_0 \frac{I_{\mathrm{pump}}^2 [1 - \exp(-\alpha_{\mathrm{THz}} L)]^2}{\alpha_{\mathrm{THz}}^2} \quad (1)$$

where C_0 is a constant. Due to the generation of the free carriers by the pump laser a significant fraction of the THz power can be absorbed by the photogenerated carriers. Therefore, the THz absorption coefficient can be approximately written as $\alpha_{\mathrm{THz}} \approx \alpha_0 I_{\mathrm{pump}}$, where α_0 is a constant. Under such an assumption, we can use equation (1) to fit the data presented in figure 4. One can see from figure 4 that we have obtained a good agreement between our model described by equation (1) and data. Following the nonlinear least-squares fitting, we have obtained the value for $\alpha_0 L$ to be 8.31 cm^2 kW^{-1}. This implies that if the pump intensity is much lower than $(\alpha_0 L)^{-1} \approx 120$ W cm^{-2}, the THz output power should be proportional to the square of the pump intensity. However, when the pump intensity is close to 120 W cm^{-2}, the power dependence starts to deviate from the square law. Such a predicted behavior is indeed consistent with our measurement shown in figure 4.

According to our theoretical model described by equation (1), the maximum THz power generated from sample 2 is 3.89 μW. Due to the strong saturation of the output power as the pump intensity is increased, even at the pump intensity of 600 W cm^{-2}, the THz output power has already reached 3.84 μW, which is just about 1% below the maximum value of 3.89 μW. In the future, we plan to explore the regime of the strong saturation of the output power at the pump intensities of much higher than 120 W cm^{-2}.

In order to find out the exact mechanism for the THz generation in these two series of the InN thin films, we have measured the dependences of the THz output power and polarization angle on the pump polarization angle at the incident angle of $\theta \approx 64°$, respectively, see figures 5 and 6. Let us assume that the optical rectification induced through second-order nonlinearity is the only mechanism for the THz generation observed in our InN films. According to [9], the THz output power should be proportional to the square of the effective second-order nonlinear coefficient, i.e. $d_{\mathrm{eff}}^2 = (d_y \cos\alpha + d_z \sin\alpha)^2 + d_x^2$, where α is the internal angle of the pump beam inside the InN film. After taking into the consideration the Fresnel loss at the air–InN interface, d_x, d_y, and d_z can be defined as follows:

$$\begin{aligned} d_x &= 2d_{31}(\cos\varphi \sin\varphi \sin\alpha) t_p t_s \\ d_y &= 2d_{31}(\cos^2\varphi \cos\alpha \sin\alpha) t_p^2 \\ d_z &= d_{31}(\sin^2\varphi) t_s^2 + d_{31}(\cos^2\varphi \cos^2\alpha) t_p^2 + d_{33}(\cos^2\varphi \sin^2\alpha) t_p^2 \end{aligned} \quad (2)$$

where φ is the angle of the pump polarization formed with respect to the incident plane, see the inset in figure 3, and t_p

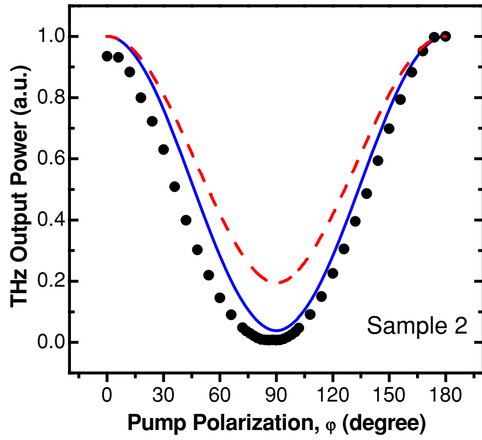

Figure 5. Normalized THz output power versus the pump polarization angle. Solid curve: theoretical results by including optical rectification and photocurrent surge. Dashed curve: theoretical results without taking into consideration photocurrent surge.

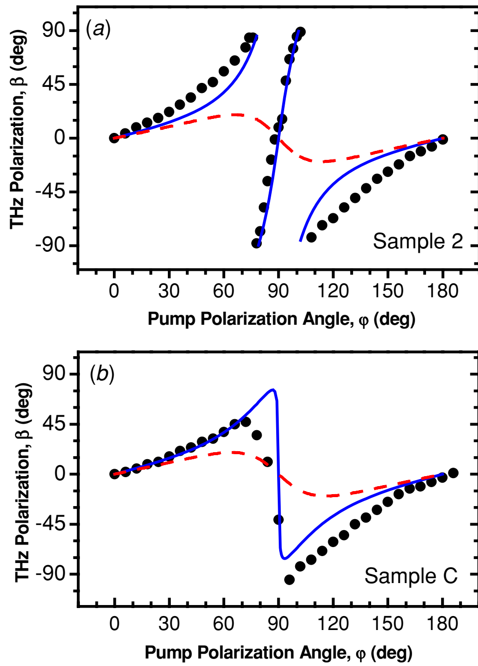

Figure 6. THz polarization versus the pump polarization angle for (*a*) sample 2 and (*b*) sample C. Dots: experimental results. Solid curves: theoretical results by including optical rectification and photocurrent surge. Dashed curves: theoretical results without taking into consideration photocurrent surge.

and t_s are the amplitude transmittance of pumping *p*- and *s*-polarization, respectively. We also want to impose the condition: $d_{33} = -2d_{31}$ [14] and use an estimated value of 2.45 as the index of refraction for the InN film at 782 nm [15]. We have then plotted the theoretical curves for the THz generation from the InN films, see figures 3, 5 and 6 (i.e. the dashed curves). One can see that the optical rectification alone cannot be used to explain the near-zero output powers when the pump polarization angle is around 90°, see figure 5. Furthermore, our theory based on the optical rectification only cannot be used to explain the large jumps of the THz polarization angles as the pump polarization angle is increased, see figures 6(*a*) and (*b*). Even for the dependence of the THz output power on the incident angle, illustrated by figure 3, one can clearly see the obvious deviation of the data from our theoretical curve when the incident angle $|\theta| > 20°$.

In order to understand the origin for the discrepancies between the data and our theoretical curves, we have included the possible contribution originating from the photocurrent surge to the THz generation. Since a large amount of electrons are accumulated near the InN surface as a result of the band-bending effect, a strong build-in electric field is present. According to [16], the direction of such a built-in electric field points to the surface normal of the InN film. Consequently, the drift of photogenerated electrons under such a build-in electric field toward the substrate may contribute to the THz radiation from each InN film. Similarly, the diffusion of the electrons away from the surface could also contribute to the THz radiation from the InN film. We have used the term 'photocurrent surge' to designate the contributions originating from the drift and diffusion of the electrons. Since the diameter of the pump laser beam is relatively large, we have neglected the effect of the carrier diffusion within the plane of the InN film. Based on equation (2), the THz polarization can be written as [6]

$$\begin{aligned} P_p &= d_{\text{eff},p}|E|^2 + d_J|E|^2 \sin\alpha \\ P_s &= d_{\text{eff},s}|E|^2 \\ \beta &= \arctan(P_s/P_p) \end{aligned} \tag{3}$$

where the $d_{\text{eff},p}$, $d_{\text{eff},s}$, d_J and β are the effective second-order nonlinear coefficients for inducing p- and s-polarizations at the THz frequencies, pseudo-nonlinear coefficient induced by photocurrent surge, and polarization angle of the THz radiation, respectively. Once P_p and P_s are determined from equation (3) above, we can then determine the magnitude of the polarization at the THz frequencies by using the expression of $P_{\text{THz}} = \sqrt{P_p^2 + P_s^2}$. Using this expression whereby P_p and P_s are given by equation (3) and the expression for β, see equation (3), we have carried out the nonlinear least-squares fitting to our data in 5 and 6 (indicated by the solid curves).

As a result of the fitting, we have obtained $d_J = -0.10\, d_{31}$ and $d_J = -0.12\, d_{31}$ for sample C and sample 2, respectively. It is worth noting that the value of d_J for sample 2 is about 20% higher than that for sample C. This may be caused by the increase in the nonradiative recombination rate of the photogenerated carriers in sample 2. As a result, the screening of the built-in electric field by the photogenerated carriers is significantly reduced. One can see from figures 5 and 6 that after including the contribution from photocurrent surge, the fitting to our data by using our theoretical model has been significantly improved. Using the values of d_J obtained from the fitting, we have fitted the dependence of the THz output power on the incident angle, see figure 3. One can see from figure 3 that the fitting has been significantly improved for the incident angles of $|\theta| > 20°$. Based on the fitting, we conclude that the photocurrent surge significantly contributes to the THz radiation from the InN films. Since d_J is opposite to d_{31}, the corresponding electric field in each InN film points to a direction being an opposite of the direction

of the pump polarization. This was previously reported in [17]. Consequently, the photogenerated electrons either drifting under such an electric field or diffusing away from the surface generate the THz radiation partially canceling out that generated by optical rectification, i.e. the destructive interference between the THz electric fields originating from photocurrent surge and optical rectification. For example, at the pump intensity of 176 W cm^{-2}, the photocurrent surge has caused the THz output power to decrease by 41% and 47% for sample C and sample 2, respectively.

Although the thickness of the InN films grown by PAMBE is about five times greater than that of the MOCVD-grown films, the THz output powers do not scale up with the thickness. It is worth noting that the absorption length of the laser beam by each InN film is about several hundred nanometers. Therefore, the InN films with the thickness of 1 μm may cause significantly higher absorption of the THz radiation generated by the films due to the presence of the high-density free carriers. We believe that this may be the primary reason why we have achieved the highest output power from one of the MOCVD-grown InN films.

In conclusion, we have investigated the dependences of the THz output power and THz polarization on the pump polarization in two series of the InN samples grown by MOCVD and PAMBE. These broadband THz pulses, with their frequencies in the range of 300 GHz–2.5 THz, were generated by ultrafast laser pulses at 782 nm. Following our analyses, we have proposed the destructive interference that between the optical rectification induced by second-order nonlinearities and photocurrent surge as the dominant mechanism for the THz generation. The highest output power achieved by us so far is 2.4 μW at an average pump intensity of 176 W cm^{-2} from the 220 nm thick MOCVD-grown InN film. This output power is significantly higher than the previous value for a similar thickness of the film.

Acknowledgment

This work has been supported by U.S. Air Force Research Laboratory, ARL-Lehigh Cooperative Agreement and National Science Foundation (DMR # 0907260).

References

[1] Yang K H, Richards P L and Shen Y R 1971 *Appl. Phys. Lett.* **19** 320
[2] Xu L, Zhang X-C and Auston D H 1992 *Appl. Phys. Lett.* **61** 1784
[3] Blanchard F *et al* 2007 *Opt. Express* **15** 13212
[4] Yeh K L, Hoffmann M C, Hebling J and Nelson K A 2007 *Appl. Phys. Lett.* **90** 171121
[5] Sarukura N, Ohtake H, Izumida S and Liu Z 1998 *J. Appl. Phys.* **84** 654
[6] Mu X, Ding Y J and Zotova Y B 2007 *Opt. Lett.* **32** 3321
[7] Ascázubi R, Wilke I, Denniston K, Lu H and Schaff W J 2004 *Appl. Phys. Lett.* **84** 4810
[8] Chern G D, Readinger E D, Shen H, Wraback M, Gallinat C S, Koblmüller G and Speck J S 2006 *Appl. Phys. Lett.* **89** 141115
[9] Mu X, Ding Y J, Wang K, Jena D and Zotova Y B 2007 *Opt. Lett.* **32** 1423
[10] Mu X, Zotova I B and Ding Y J 2008 *IEEE J. Sel. Top. Quantum Electron.* **14** 315
[11] Jamil M, Zhao H, Higgins J and Tansu N 2008 *Phys. Status Solidi* A **205** 2886
[12] Jamil M, Zhao H, Higgins J and Tansu N 2008 *J. Crys. Growth* **310** 4947
[13] Jamil M, Arif R A, Ee Y K, Tong H, Higgins J B and Tansu N 2008 *Phys. Status Solidi* A **205** 1619
[14] Levine B F 1973 *Phys. Rev.* B **7** 2600
[15] Jiang L F, Shen W Z, Yang H F, Ogawa H and Guo Q X 2004 *Appl. Phys.* A **78** 89
[16] Mahboob I, Veal T D, McConville C F, Lu H and Schaff W J 2004 *Phys. Rev. Lett.* **92** 036804
[17] Liang W, Tsen K T, Ferry D K, Lu H and Schaff W J 2004 *Appl. Phys. Lett.* **84** 3681